INTERNATIONAL JOURNAL OF AUTOMOTIVE SCIENCE AND TECHNOLOGY

2026, VOL. 10, NO:2, 427-436 www.ijastech.org e-ISSN: 2587-0963

Evaluation of a VIPV-Based Solar-Assisted Charging System with Multi-MPPT Control and Shingled PV Panels for Electric Urban Delivery Motorcycles

Ahmet Hamdi Aksoy[1], Ahmet Necati Özsezen[2,3*], Talat Özden[1]

[1.] *ODTÜ-GÜNAM, Middle East Technical University Solar Energy Research and Application Center, 06800, Çankaya-Ankara, Türkiye*
[2.] *Department of Automotive Engineering, Faculty of Technology, Kocaeli University, 41001, İzmit-Kocaeli, Türkiye*
[3.] *AYARGEM, Kocaeli University, 41001, İzmit-Kocaeli, Türkiye*

Abstract

This study presents the systematic design, multi-surface integration, and experimental validation of a Vehicle-Integrated Photovoltaic (VIPV) system tailored for an electric urban delivery motorcycle. To maximize power density within highly constrained vehicular surface areas, a high-density shingled cell architecture was developed to elevate string voltage and optimize conversion efficiency. Ethylene Tetrafluoroethylene (ETFE) was used as a lightweight front-sheet material, providing more stable efficiency yields compared to standard Polyethylene Terephthalate (PET)-coated alternatives under fluctuating environmental conditions. To mitigate severe mismatch losses caused by the multi-oriented geometry of the courier delivery box, a multi-channel Maximum Power Point Tracking (MPPT) architecture was commissioned to independently manage heterogeneous irradiance profiles. Real-world outdoor testing conducted in Ankara, Türkiye, over a cumulative active test duration of 40,980 seconds (~11.4 hours), demonstrated a cumulative energy harvest of 364.9 Wh. This solar gain successfully yielded a 20.3% increase in the battery State-of-Charge (SoC) and provided an additional grid-independent driving range of approximately 14.2 km. Despite efficiency fluctuations induced by dynamic urban shading, the integration of flexible shingled PV panels with a tailored power electronics topology represents a promising approach to enhance the sustainability and range autonomy of lightweight electric mobility.

Keywords: Electric motorcycle; Vehicle-integrated photovoltaics (VIPV); Shingled PV modules; multi-maximum power point tracking (MMPPT); PV mobility monitoring systems.

Research Article

History
Received 28.03.2026
Revised 11.06.2026
Accepted 16.06.2026

Contact
* Corresponding author
Ahmet Necati Özsezen
nozsezen@kocaeli.edu.tr
Address: Automotive Engineering Department, Faculty of Technology, Kocaeli University, 41001, Kocaeli, Türkiye
Tel:+902623032317

To cite this paper: Aksoy, A.H., Özsezen, A.N., Özden, T. Evaluation of a VIPV-Based Solar-Assisted Charging System with Multi-MPPT Control and Shingled PV Panels for Electric Urban Delivery Motorcycles. International Journal of Automotive Science and Technology. 2026; 10(2): 427-436. https://doi.org/10.30939/ijastech..1917959

1. Introduction

The electrification of transportation stands as a pivotal strategy for mitigating air pollution in densely populated regions, offering a transformative path toward energy diversification and significant decarbonization; while hybrid systems offer a notable reduction in carbon emissions, fully electric vehicles (EVs) can achieve emission reductions of up to 32.5%[1]. In the context of Türkiye's major metropolises, characterized by chronic traffic congestion and inefficient 'stop-and-go' driving cycles, EVs emerge as a critical solution to eliminate tailpipe emissions at the source [2]. Beyond achieving zero local emissions, EVs provide substantially higher energy efficiency compared to internal combustion engine vehicles, particularly when integrated with a low-carbon power grid. This transition not only reduces fossil fuel dependency and urban noise levels but also positions EVs as a fundamental pillar of the smart city ecosystem through potential ancillary services to the energy grid. [3–5].

Particularly in the rapidly expanding urban logistics and last-mile delivery sectors, electric motorcycles have become a strategic alternative due to their silent operation and low operating costs. Life cycle assessments indicate that despite higher initial investment costs, these vehicles offer a lower total cost of ownership through significantly reduced maintenance and operational expenses. However, their widespread adoption is still hindered by critical constraints, namely limited battery capacity and inadequate charging infrastructure. These frequent charging requirements increase grid dependency and accelerate battery degradation, ultimately undermining the system's overall sustainability. [6,7].

Integrating vehicle-integrated photovoltaic (VIPV) systems into two-wheeled light electric vehicles offers a promising

solution to these challenges by enhancing delivery efficiency and, most importantly, extending the operational range[8]. By leveraging the available surface area for on-board energy generation, reliance on external charging can be minimized. Driven by these motivations, this study presents a novel conceptual design and performance analysis for a motorcycle-integrated photovoltaic system, as illustrated in Figure 1.



Figure 1. The concept design of the electric urban delivery motorcycle

Vehicle-Integrated Photovoltaic (VIPV) systems offer transformative potential to partially fulfill the energy demands of electric vehicles, effectively extending their operational range while mitigating reliance on external charging infrastructure. While existing literature extensively documents PV-assisted concepts for passenger cars, experimental research specifically targeting electric motorcycles, particularly those featuring complex, multi-surface geometries, remains notably sparse. On compact platforms such as motorcycles, surfaces with diverse orientations are subjected to non-uniform irradiance levels, which frequently leads to significant mismatch losses in power generation[9,10].

Despite these structural challenges, the reported benefits of VIPV integration are substantial. Current technologies demonstrate a significant potential to extend driving range; for instance, Samadi et al.[11] reported that vehicle-integrated photovoltaic systems can provide an additional annual range of 1700–5500 km for buses, 650–5000 km for minibuses, and 840–6180 km for luggage tractors. Furthermore, VIPV systems can reduce both charging time and charging frequency by up to 16% [12,13], while gradual VIPV charging can further reduce grid charging frequency by up to 23% [8], highlighting their practical advantages in real-world applications.

Beyond irradiance variability, the relatively high charging voltage requirements of electric vehicle battery systems impose a major engineering constraint on onboard PV design [14]. In conventional module architecture, the limited surface area often results in an output voltage that is substantially lower than the battery voltage[15]. This discrepancy necessitates high step-up ratios in the power electronics stage, requiring high-gain boost converters that inevitably increase switching and transmission losses, thus compromising overall system efficiency [16].

To circumvent these limitations, this study employs shingled cell technology. By overlapping laser-cut cell strips, the shingled architecture enables a higher density of cells to be integrated into a single module, resulting in elevated string voltages and reduced operating currents. This configuration not only minimizes resistive losses but also significantly enhances module resilience under partial shading conditions[17]. Consequently, shingled modules facilitate a higher average output voltage, which effectively reduces the required voltage gain from the boost converter and optimizes the energy conversion efficiency of the entire VIPV system.

When implementing PV integration on a multi-surface electric motorcycle, the weight of the encapsulation material becomes a critical design parameter. While conventional glass-covered modules offer high mechanical durability, they impose an undesirable increase in vehicle mass, which negatively impacts the energy consumption and operational range of lightweight two-wheelers. Consequently, replacing glass with lightweight, high-transparency, and weather-resistant alternatives is essential for vehicular efficiency. Ethylene Tetrafluoroethylene (ETFE)[18] stands out as an ideal polymer for VIPV applications due to its low density, superior optical transmittance particularly in the visible and near-infrared spectrum and exceptional UV resistance. Furthermore, its inherent hydrophobic surface characteristics contribute to maintaining highlight transmittance by minimizing the accumulation of dust and environmental soiling [5].

To address the challenge of non-uniform irradiance caused by the varying orientations of motorcycle-mounted photovoltaic surfaces, a Multi-Maximum Power Point Tracking (MMPPT) strategy was adopted. Under such conditions, individual PV strings operate at different local maximum power points, making centralized MPPT control unable to simultaneously optimize the performance of all modules. Previous studies have demonstrated that MMPPT architecture, which employ independent tracking units for each PV string, can significantly improve energy harvesting efficiency in distributed photovoltaic systems exposed to multiple local maxima [6, 7].

Although several studies have investigated VIPV applications for passenger cars, buses, and other larger electric vehicles, experimental investigations focusing on electric urban delivery motorcycles remain extremely limited. Moreover, the combined application of lightweight ETFE-encapsulated shingled photovoltaic modules together with an independent MMPPT architecture for managing non-uniform irradiance on multiple vehicle surfaces has not been sufficiently addressed in the literature. Therefore, the originality of the present study lies in the development and experimental validation of a VIPV-assisted electric delivery motorcycle specifically designed to maximize onboard solar energy harvesting under real operating conditions. In the proposed system, elevated string voltage shingled PV modules,

lightweight ETFE encapsulation, and independent MPPT controllers for each photovoltaic surface were utilized together to minimize mismatch losses and elevate overall energy conversion efficiency. In addition, this study aimed to provide valuable insights to the emerging field of photovoltaic-assisted light electric mobility by presenting experimental data regarding harvested energy, charging performance, and potential range extension.

2. Design of the Electric Delivery-Type Motorcycle

2.1. System Platform and Baseline Characterization

The experimental study was conducted using a commercially available electric motorcycle equipped with a 2-kW brushless DC (BLDC) traction motor and a 72 V, 25 Ah lead-acid battery pack. This specific vehicle was selected due to its operational characteristics representing urban "last-mile" delivery applications and its adequate surface area suitable for the integration of auxiliary PV charging systems.

Prior to the installation of the PV modules, the system's baseline energy consumption and battery discharge performance were extensively characterized to establish reference operating conditions. The comprehensive schematic of experimental system architecture, specifically optimized for urban courier operations, is illustrated in Figure 2.

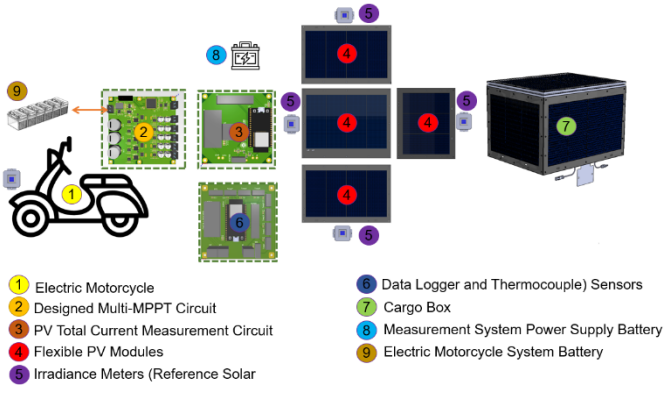


Figure 2. The schematic representation of the experimental system

2.2 Design of the Flexible Photovoltaic Shingled-Type Panels and Indoor Performance Tests

The module fabrication process begins with the precision laser-cutting of full-sized solar cells into narrow strips. These resulting shingled cells allow for a more compact and high-density layout by reducing shading losses. The stringing process was performed using a custom-designed automated "shingled cell stringing and adhesive dispensing" machine. This system minimizes manufacturing defects which could otherwise impair module performance by precisely controlling the overlap ratio between cells and the amount of conductive adhesive applied.

In the shingled cell design, full-sized square PERC cells (M2 Size) are typically divided into five cell strips via laser cutting. These cells were produced at the ODTÜ GÜNAM Photovoltaic Line (GPVL). The size of each strip depends on the number of transverse busbars of the original cell (e.g., they can be cut into 5-busbar configurations). The cutting process is generally performed through the center or edge of the front-surface conductive busbars; thus, each resulting strip features a front-surface busbar residue on one end and a rear-surface conductive area (metal contact) on the other. These cell strips are aligned in the same orientation and overlapped such that the front busbar region of one strip sits atop the rear-surface of the preceding strip.

To prevent the rear contact from causing excessive shading on the cell during stringing, the offset distance is calculated for maximum efficiency. This distance is defined by considering the combined effect of the total cell strip length (d) and geometric parameters: distance to the busbar (a), busbar width (b), and rear contact length (c). This parameter is calculated to ensure optimum electrical contact in the overlapping region while preventing unnecessary shading, as mathematically expressed in Eq. (1) and illustrated in Figure 3.

$$x_{offset} = d - \left(\frac{c}{2} + \frac{b}{2} + a\right) \quad (1)$$

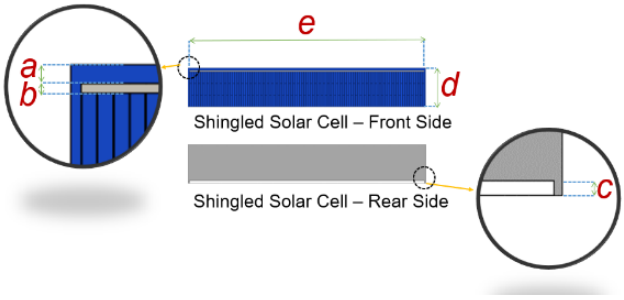


Figure 3. Schematic representation of the front and rear sides of a shingled solar cell and its geometrical parameters.

Electrical connection is established via Electrically Conductive Adhesive (ECA) applied between these overlapping contact areas. Consequently, each cell strip is connected in series to its adjacent strip. In the shingle arrangement, the overlap between neighboring segments is typically determined by the offset; this amount is defined according to the busbar width, distance to the busbar, rear contact width, and cell size, aiming to fully cover the busbars without creating shadows. The minimum overlap ratio (*Overlap Ratio (%)* $_{min}$) for overlapping shingled cells is expressed as Eq. (2).

$$Overlap\ \ Ratio\ \ (\%)_{min} = \frac{a+\frac{b}{2}+\frac{c}{2}}{d} x\ \ 100 \quad (2)$$

While a lower overlap ratio can increase module efficiency by maximizing the active area, an excessively low overlap may

reduce the contact area provided by the adhesive, thereby increasing series resistance. Furthermore, it can lead to adhesive overflow or short internal circuits. Therefore, the optimum overlap ratio is determined by balancing both electrical performance and mechanical integrity

Table 1. Structural layer specifications and material properties of the shingled PV modules

Layer	Material	Thickness	Tolerance
Front-sheet (Option 1)	ETFE	0.025 mm	±0.003 mm
Front-sheet (Option 2)	PET	0.315 mm	—
Upper Encapsulant	EVA	0.45 mm	—
Cell	Shingled Cell	180 µm	±20 µm
Lower Encapsulant	EVA	0.45 mm	—
Backsheet	Polymer Backsheet	0.315 mm	±5%

The module structure consists of a 0.025 mm ETFE front-sheet and 0.45 mm EVA as the protective encapsulant. After the cell strings were positioned, a rear EVA embedding layer and a final backsheet were laminated in sequence to complete the module architecture. The detailed layer structure is presented in Table 1. Figure 4 present a schematic representation showing the layer configuration and key production steps of the light-weight, glass-free shingled PV module developed for VIPV applications.

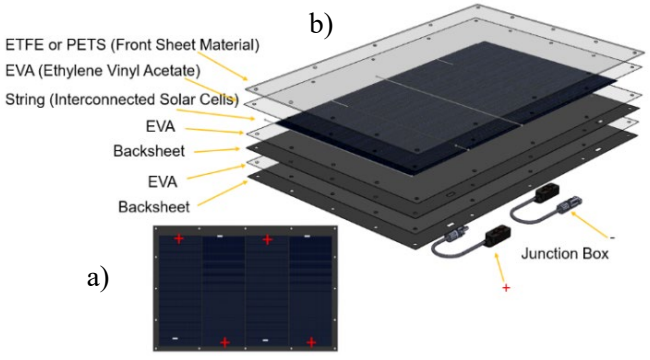


Figure 4. Shingled PV panels (a) Front view and electrical polarity layout of the shingled PV module, (b) Exploded view showing the layered structure and material components of the flexible shingled PV panel.

The laser-cut cell strips are sequentially overlapped using ECA via the in-house developed automation system. Unlike conventional soldering methods, this bonding architecture limits thermal stress, minimizing the risk of micro-cracks. These shingled cell strings, which undergo a curing process to optimize mechanical stability and electrical conduction, form the core energy-generating layer of the module.

During lamination, this core structure is enclosed by EVA layers from both top and bottom to ensure homogenous pressure distribution and enhanced mechanical durability. The outermost back sheet protects the cells against environmental factors such as moisture, mechanical impact, and thermal fluctuations while completing the electrical insulation of the system.

The lamination process was carried out under specific vacuum and pressure values to preserve the structural integrity of the modules and the cell architecture. The air pressure was kept constant at 0.525 MPa; to extract air between layers and achieve a bubble-free structure, the upper vacuum was maintained at -91.8 kPa, and the lower vacuum at -92.2 kPa. This vacuum balance ensures that the ETFE (or the economical PET alternative) front-sheet adheres uniformly to the cell surface, optimizing thermal and mechanical stability. The process concluded with the assembly of the junction box, followed by Electroluminescence (EL) imaging and I-V performance tests.

Electrical performance measurements of the completed modules under Standard Test Conditions (STC) (including I_{sc}, V_{oc}, and Efficiency) are detailed in Table 2. Additionally, structural integrity and post-production cell quality are presented through the EL images in Figure 5.

Table 2. STC Performance Parameters of Shingled PV Modules

Surface	Right Side	Top	Left Side	Rear
Short Circuit Current I_{sc} (A)	1.69	1.68	1.61	1.71
Short Circuit Voltage V_{oc} (V)	33.93	38.6	33.68	25.16
Rated Power P_{max} (W)	43.85	49.92	41.81	32.33
Rated Current I_{mpp} (A)	1.58	1.53	1.51	1.58
Rated Voltage V_{mpp} (V)	27.77	32.65	27.72	20.48
FF (%)	76.42	76.96	77.11	75.14
PV module Efficiency (%)	19.45	19.61	18.55	19.12
Surface Area (m^2)	0.2205	0.257	0.2205	0.1659
Front Material	ETFE	ETFE	PET	ETFE

A comparison between the left and right-side modules (Panels 2 and 3, respectively), which have the same surface area, shows the impact of material selection on performance. Although the ETFE-coated shingled PV module had a short-circuited cell, it achieved higher efficiency compared to the equivalent PET-coated module. Due to this performance difference and the optical advantages of ETFE, ETFE was used as the primary encapsulant material for subsequent stages of the study.

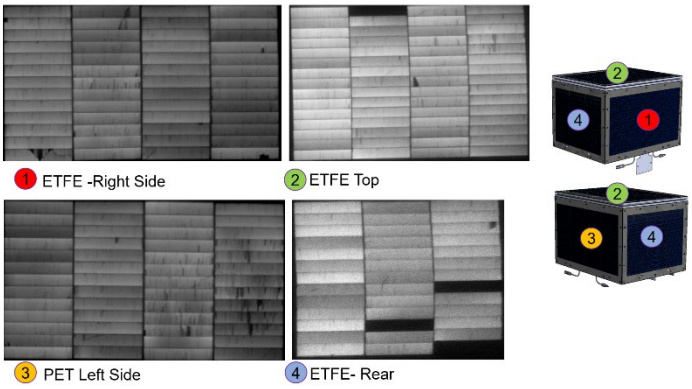


Figure 5. Electroluminescence (EL) results show structural integrity, cell defects, and the surface-specific integration layout of the four shingled PV panels.

.3. Electrical Architecture and MPPT Integration

The PV system is integrated into the vehicle's energy storage unit through a multi-channel Maximum Power Point Tracking (MPPT) architecture, specifically designed to charge the battery pack with an 82V output. The electrical infrastructure comprises a high-efficiency PV array with a total capacity of 167 Wp and a programmable MPPT controller based on an STM32 microcontroller. Although the control unit was hardware-designed with a 5-channel modular structure, four channels (Rear, Top, Right, and Left) were actively commissioned, as the front panel was not installed during the application phase.

During the transition from theoretical design to physical implementation, critical hardware limitations were encountered, particularly regarding the high boost ratio required to step up the input voltage (20–32V) to the target 82V. In the initial prototypes, CF199 Green Ferrite cores were utilized. Due to their lack of an air gap, these cores reached magnetic saturation at a very low current level of approximately 0.30 A. This caused the inductor to lose its characteristic impedance and behave like a simple conductor, pushing the circuit toward a short-circuit mode. Consequently, excessive thermal stress occurred on the MOSFET switching elements, leading to overall system instability.

To overcome this magnetic saturation issue, high-performance black Kool Mμ MAX (79617A7) cores with a distributed air gap structure were selected for the inductor design. This core structure, providing 189 nH/T² inductance, offered the desired saturation limit under 100 turns, thereby maintaining magnetic stability even at maximum panel currents of approximately 1.7 A. At a switching frequency of 25 kHz, the target input current ripple ratio ($r = \Delta I / I_{in}$) was maintained at 10%. Despite the required duty cycles, the system remained in Continuous Conduction Mode (CCM) thanks to inductance values specifically calculated for each panel orientation (see Table 3), ranging between 1.93 mH and 2.28 mH.

Table 3. Operating characteristics and Maximum Power Point (MPP) parameters of the integrated shingled PV panels under real-world conditions.

Panel Location	Rear	Top	Side (Right)	Side (Left)
Front-sheet	ETFE	ETFE	ETFE	PET
I_{out} (A)	0.394	0.609	0.535	0.51
Duty cycle (%)	76.8	63	68.5	68.6
L (mH)	2.28	1.93	2.03	2.13
C (μF)	14.8	18.7	17.9	17.1

The dynamic control of the system is governed by the Perturb and Observe (P&O) algorithm, detailed in Figure 6. This algorithm continuously analyzes instantaneous power fluctuations and voltage variations to update the reference voltage, stabilizing the system at the maximum power point. The electrical schematic of the designed multi-channel MPPT system, the operating points on the I-V/P-V curves, and the physical prototype are presented in Figure 7. These optimizations contributed to the preservation of battery life and ensured stable converter efficiency even under fluctuating solar irradiance conditions.

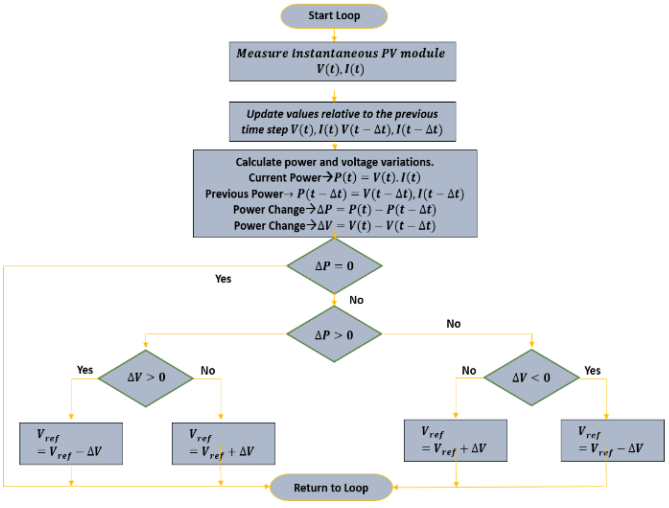


Figure 6. Flowchart of the multi-channel Perturb and Observe (P&O) control algorithm optimized for the VIPV system

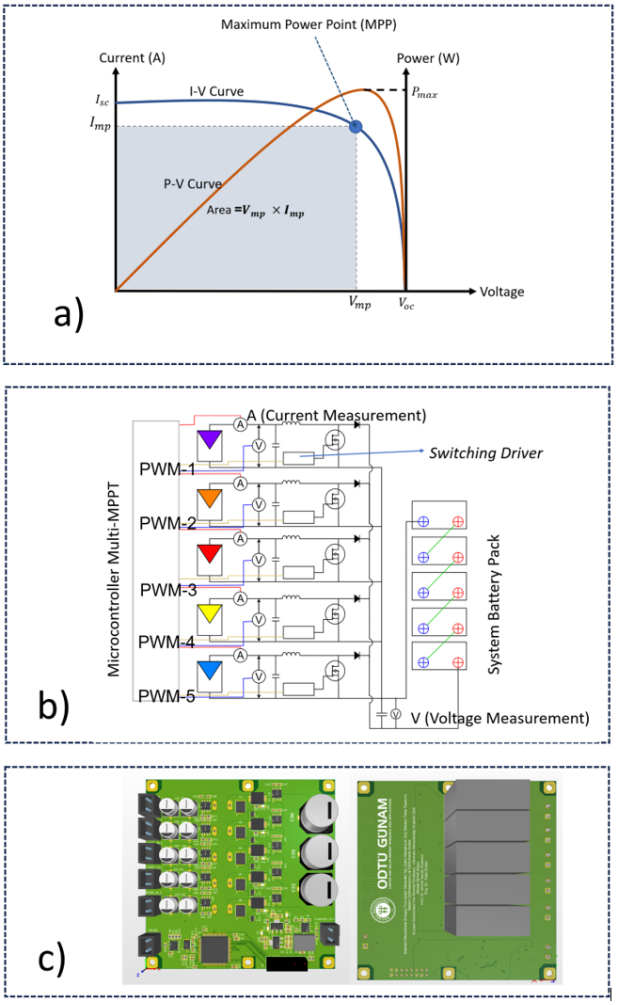


Figure 7. Multi-input VIPV charging system implementation (a) PV module I-V and P-V characteristic curves, (b) Schematic layout of the multi-channel MPPT control unit (boost MPPT topology), (c) Final hardware assembly and 3D PCB layout for motorcycle integration.

2.4. Design and Calibration of Irradiance Sensors

To accurately quantify the solar potential across the motorcycle's multi-oriented surfaces, calibrated irradiance sensors (31.2 mm x 31.2 mm) were developed using PERC monocrystalline silicon cells. The structural configuration and integrated components of these functional prototypes are illustrated in Figure 8. These sensors are designed to measure both the instantaneous global irradiance and the effective irradiance converted by the PV modules, enabling a high-fidelity, surface-specific radiation assessment.

To ensure environmental durability and optical stability, the sensors feature a multi-layer encapsulation comprising high-transmittance glass, EVA, and a protective back sheet. The electronic architecture (Figure 8b) integrates a 24-bit ADS1220 programmable gain amplifier (PGA) for signal acquisition, an ESP32 microcontroller, and a sensor for real-time temperature compensation. Data transmission is executed via an RS485/RTU Modbus interface to provide immunity against high-frequency noise typically present in electric vehicle environments.

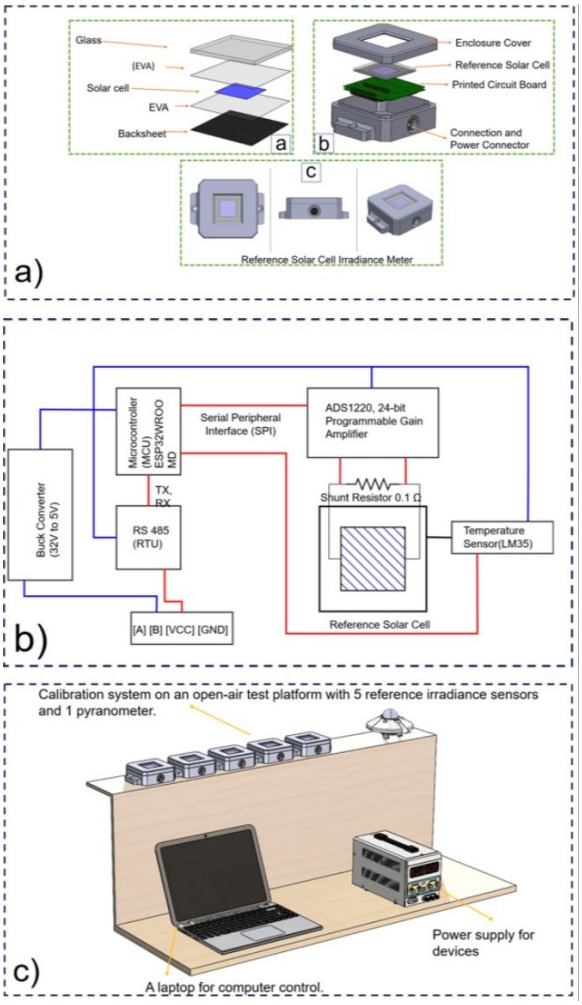


Figure 8. Structural layers and housing (a) Design of the reference solar cell irradiance meter, (b) Electronic circuit block diagram featuring ESP32 and ADS1220, (c) Outdoor calibration setup with a reference pyranometer and computer-controlled data acquisition system.

The outdoor calibration process was conducted using a SMP11 pyranometer as a reference standard on a synchronized open-air test platform (Figure 8c). The experimental data verified sensor performance across a range of irradiance levels and cell temperatures from 20°C to 60°C. Statistical analysis, presented in Figure 9, shows linearity with R^2 values exceeding 0.997 for all units. Calibration equations derived for each sensor were used to maintain accuracy during dynamic driving tests.

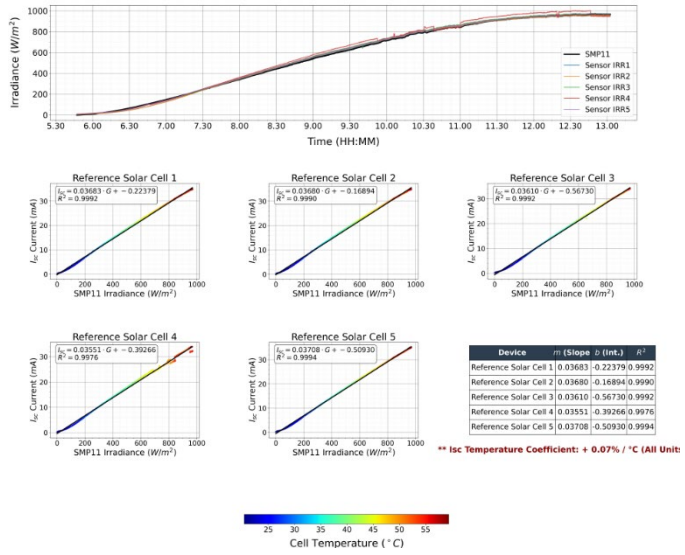


Figure 9. Calibration curves, time-dependent irradiance measurements, and linear regression analysis of the developed reference solar cell sensors.

2.5. Measurement and Data Acquisition System

A measurement and data acquisition (DAQ) infrastructure was set up to evaluate the real-time performance of the integrated system. This setup enables synchronous recording of electrical parameters from the photovoltaic panels together with environmental variables. The system includes four custom reference-cell-based irradiance sensors to monitor solar potential on each surface. A seven-channel data logger was used to track thermal profiles, including PV panel surface temperatures and power electronics component temperatures. Thermal data were collected using K-type thermocouples, which are suitable for outdoor use.

The electrical characteristics from the PV strings were transmitted via an RS485 (RTU Modbus) communication interface. This data was then combined with environmental variables and stored on an SD card. A Real-Time Clock (RTC) module was used to keep time information during dynamic driving tests.

3. Result and Discussion

In this study, the performance of the VIPV system integrated into the delivery box of the electric motorcycle was experimentally evaluated in Ankara, Türkiye, in September on a selected 20 km route while driving and while parked. The system behavior under dynamic shading, variable solar irradiance, and temperature effects was examined.

Measurements taken under driving conditions showed that irradiance distribution over the delivery box surfaces varies with time and orientation. The top, rear, right, and left surfaces experience distinctly different irradiance profiles due to changing sun angles, dynamic shading from surrounding buildings, and changes in vehicle direction. Figure 10 summarizes the system's performance characteristics under these variable conditions.

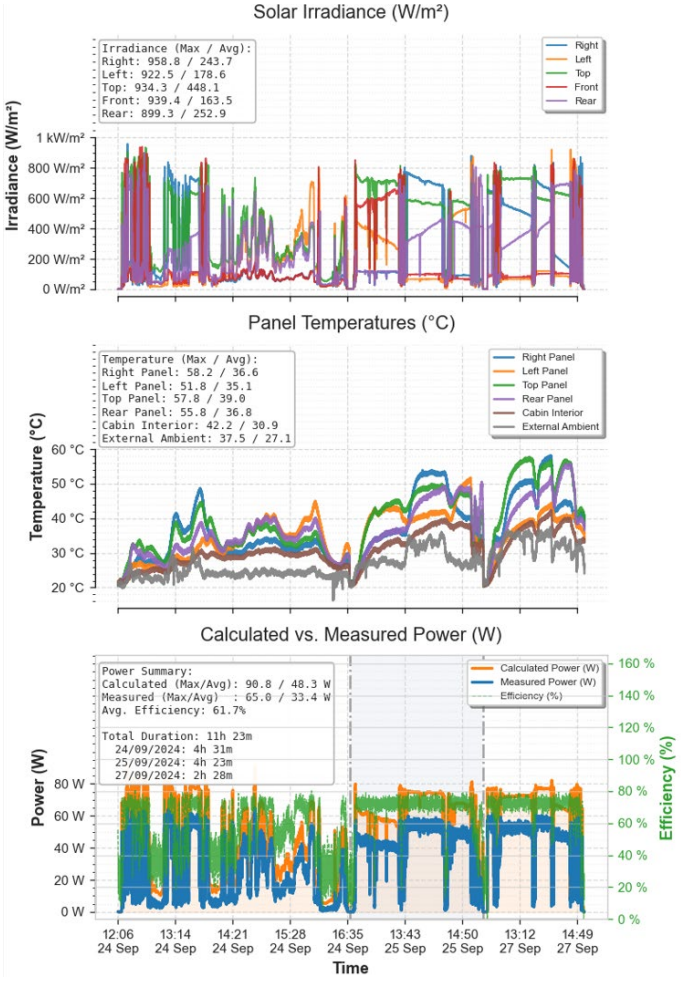


Figure 10. Performance characterization of the motorcycle-integrated PV system (a) Dynamic solar irradiance profiles across multi-oriented surfaces (front, rear, top, and sides) (b) Operational temperature variations of the PV panels during the test cycle (c) Correlation between theoretical power (derived from irradiance) and actual power delivered to the battery.

The comparative analysis of average solar irradiance on different surfaces of the delivery box is presented in Table 4. The data show variation in energy potential depending on surface orientation. The top surface received the highest average irradiance at 448 W/m², accounting for 45.1% of the total radiation captured. This is mainly due to its horizontal orientation, which increases the sky view factor and reduces cosine losses. The rear surface and the right side had similar irradiance levels of 253 W/m² (18.3%) and 244 W/m² (21.9%), respectively. The left side recorded the lowest value at 179 W/m² (14.7%), which may be due to shading or its orientation relative to the sun during the test cycle. These results indicate that the top of the delivery box is a suitable area for PV integration to support the vehicle's energy needs.

Table 4. Comparative analysis of average solar irradiance on courier box surfaces

Courier Box Surface	Average Irradiance (W/m^2)	Distribution Share	Technical Remark
Top	448	45.1%	Highest exposure due to horizontal sky view.
Rear	253	18.3%	Moderate exposure, often influenced by the rider's shadow.
Right	244	21.9%	Significant lateral irradiance was captured during the route.
Left	179	14.7%	Lowest exposure, likely due to shading or route orientation.
Total	**1124**	**100%**	

This pronounced disparity highlights the critical importance of managing each surface with an independent MPPT channel in multi-surface VIPV applications. Otherwise, panels operating under low irradiance conditions can act as bottlenecks, limiting the overall system output and increasing mismatch losses, as confirmed experimentally.

The system achieved an average cycle efficiency of 61.7%. Several hardware factors influenced overall performance. The high duty cycle required to boost the input voltage (20–32 V) to the 82 V battery threshold increased conduction losses. To maintain thermal management, the switching frequency was limited to 25 kHz; exceeding this limit would increase MOSFET switching losses and thermal dissipation. As a result, the lower frequency caused higher current ripple. During low irradiance, reduced panel output current affected the stability of the MPPT algorithm, occasionally causing tracking interruptions.

The use of shingled cell architecture helped increase panel output voltage by enabling high series cell density on the limited delivery box surface. This reduced the boost ratio required at the power conversion stage. Reference cell-based irradiance sensors, which have the same spectral response as the PV panels, provided accurate measurements of effective irradiance. This allowed an objective assessment of how instantaneous shading affects system efficiency under dynamic driving conditions.

The cumulative energy generation and the corresponding range enhancement during the test period are presented in Table 5. Table 5 summarizes the numerical values from the test cycles.

Table 5. Cumulative energy generation, SoC increase, and range contribution by test day.

Date		Gen.(Wh)	Range Ext.(km)	Daily SOC (%)
24 Sept.	4h31min	106	+4.12	5.89%
25 Sept.	4h23min	145	+5.65	8.06%
27 Sept.	2h28min	114	+4.43	6.33%
Total	11h 22min	365	+14.2	20.28%

Energy harvesting effectively commenced on the first day of the experimental campaign. As detailed in Table 5, the system generated 106 Wh during the first day (4 h 31 min), 144 Wh on the second day (4 h 23 min), and 114 Wh on the third day (2 h 28 min). Over this active three-day monitoring period, the VIPV configuration achieved a cumulative energy yield of 364 Wh. Based on the vehicle's baseline consumption of ~25.7 Wh/km derived from its 1800 Wh battery (72 V, 25 Ah) and 70 km WLTP range this solar gain increased the battery State-of-Charge (SoC) by 20.3% and extended the driving range by 14.2 km independent of grid charging. The added weight of the PV panels (~2.34 kg) and other system components were excluded from these energy consumption calculations, with all parameters relying strictly on the vehicle's factory specifications.

It should be highlighted, however, that these experimental measurements were conducted within a highly restricted three-day window in September, which limits their capacity to represent comprehensive annual performance. Under shifting seasonal variations such as winter periods or prolonged overcast conditions both diminished solar irradiance levels and shortened daylight hours will inevitably degrade the cumulative energy yield. Conversely, elevated ambient temperatures during the summer season are projected to induce thermal losses, thereby reducing overall panel efficiency due to the inherent negative temperature coefficient characteristic of silicon-based photovoltaic cells. Consequently, to precisely quantify the true annual energy yield, evaluate structural trade-offs like panel weight, and establish the ultimate economic viability of such motorcycle-integrated VIPV systems, extensive and year-round field testing across diverse climatic conditions remains a critical necessity.

4. Conclusions

This study investigates the integration of a multi-surface VIPV system onto an electric urban delivery motorcycle and analyzes its effects on operational autonomy. At the end of the experimental test period, the cumulative energy generation was measured as 364.9 Wh, corresponding to a 20.3% increase in battery SoC and an additional grid-independent range of 14.2 km. The obtained data point to the potential of utilizing urban solar irradiance for mobility applications through PV systems integrated into restricted vehicle surfaces.

Technical analyses show the functionality of shingled cell technology and multi-channel MPPT strategies in compact and versatile VIPV applications. The shingled architecture increased the series cell density in limited space, elevating the string voltage and reducing the duty cycle requirements of the boost converters. The multi-channel MPPT approach limited mismatch losses resulting from heterogeneous irradiance distribution. While the top panel provided 45.1% of the total generated power, the exposure of the side and rear panels to variable shading conditions highlights the use of independent tracking architectures as an option for optimizing system efficiency.

The system exhibited a round-trip efficiency of 61.7%, despite high voltage gain requirements and thermal constraints limiting the switching frequency to 25 kHz. Allowing the converters to operate at higher switching frequencies represents another area of study for potential performance improvement. Additionally, edge passivation processes applied after cell cutting operations and the mitigation of shunt risks in electrically conductive adhesive (ECA) applications are among other parameters that may influence electrical efficiency at the cell level.

Future work focuses on alternative power electronics topologies to boost energy obtained from low-voltage solar panels in restricted areas to levels suitable for electric vehicle architectures, as well as improving converter efficiency under low-irradiance conditions. In this regard, the integration of GaN (Gallium Nitride) or SiC (Silicon Carbide) based wide-bandgap (WBG) semiconductors could be examined. Such technological modifications have the potential to enhance the energy conversion efficiency and commercial viability of motorcycle-integrated VIPV systems by enabling higher switching frequencies and reducing conduction losses.

Acknowledgment

The authors would like to express their sincere gratitude to the Middle East Technical University (METU) – Center for Solar Energy Research and Applications (GÜNAM) for their expertise in photovoltaic characterization and for providing high-precision measurement infrastructure. The authors also gratefully acknowledge the support of Kocaeli University AYARGEM Center.

Conflict of Interest Statement

The authors declare that there is no conflict of interest in the study.

CRediT Author Statement

Ahmet Hamdi Aksoy: Resources, Investigation, Conceptualization, Methodology, Data Curation, Writing - Original Draft, Writing - Review & Editing **Ahmet Necati Özsezen**: Supervision, Writing - Original Draft, Writing - Review & Editing. **Talat Özden**: Conceptualization, Methodology, Validation.

Declaration of Generative AI in the Writing Process

The authors declare that no generative AI or AI-assisted technologies were used in the preparation of this manuscript.

References

[1] Parlak BO, Yavasoglu HA. Assessment of vehicle-integrated photovoltaics: A financial and environmental perspective. Sustain Energy Technol Assess. 2024;72:104042. https://doi.org/10.1016/j.seta.2024.104042.

[2] Çetin Doğruparmak Ş, Demirarslan KO, Çavuşoğlu SV. Evaluation of Turkey's road-based greenhouse gas inventory and future projections. Appl Sci. 2025;15(13):7007. https://doi.org/10.3390/app15137007.

[3] Li Z. The electrification of transport: Key drivers, challenges, and future directions. Highlights Sci Eng Technol. 2024;121:31-35. https://doi.org/10.54097/12kcke97.

[4] International Energy Agency. Global EV Outlook 2023. Paris: IEA; 2023.

[5] Oluwalana OJ, Grzesik K. Solar-powered electric vehicles: Comprehensive review of technology advancements, challenges, and future prospects. Energies. 2025;18(14):3650. https://doi.org/10.3390/en18143650.

[6] Yamaguchi M, Nakamura K, Ozaki R, Kojima N, Ohshita Y, Masuda T, et al. Analysis for the potential of high-efficiency and low-cost vehicle-integrated photovoltaics. Sol RRL. 2023;7(8):2200556. https://doi.org/10.1002/solr.202200556.

[7] Kouzelis A, Linders K, Bandyopadhyay S, Mouli GRC. Analysis of vehicle-integrated photovoltaics and vehicle-to-grid on electric vehicle battery life. J Power Sources. 2025;631:236117. https://doi.org/10.1016/j.jpowsour.2024.236117.

[8] Smitheram M, Gatavi E. Feasibility analysis and optimisation of vehicle-integrated photovoltaic systems for sustainable transportation. World Electr Veh J. 2025;16(11):610. https://doi.org/10.3390/wevj16110610.

[9] Celi E, Minuto A, Rizzi S, Timò G, Dolara A, Avella A. Experimental platform for PV generator characterization and MPPT algorithm simulation in vehicle-integrated photovoltaic applications under real operating conditions. Sol Energy Mater Sol Cells. 2026;294:113929. https://doi.org/10.1016/j.solmat.2025.113929.

[10] Samadi H, Ala G, Brito MC, Marcon G, Romano P, Viola F. Vehicle-integrated photovoltaic for sustainable airports: A flexible framework for performance assessment. Sustainability. 2025;17(20):9246. https://doi.org/10.3390/su17209246.

[11] Tahir MU, Sangwongwanich A, Stroe DI, Blaabjerg F. Overview of multi-stage charging strategies for Li-ion batteries. J Energy Chem. 2023;84:228-241. https://doi.org/10.1016/j.jechem.2023.05.023.

[12] Mallon KR, Assadian F, Fu B. Analysis of on-board photovoltaics for a battery electric bus and their impact on battery lifespan. Energies. 2017;10(7):943. https://doi.org/10.3390/en10070943.

[13] Balakrishnan P, Lakshmanan T, Ravi R, Faqir M. Optimization of solar energy utilization for electric vehicles. In: AI-Driven Solutions for Solar Energy Efficiency, Irradiance Modeling, and PV Forecasting. Hershey, PA: IGI Global Scientific Publishing; 2026. https://doi.org/10.4018/979-8-3373-1434-1.ch012.

[14] Nukunudompanich M, Sriprapai D, Sontikaew S. Aspects of optical and thermal performances in flexible perovskite solar cells made of nanomaterials with potential for development of vehicle-integrated photovoltaics. Mater Today Proc. 2022;66(Pt 6):3163-3167. https://doi.org/10.1016/j.matpr.2022.06.397.

[15] Wu CL, Liu ZM, Wei DY, Chen JW, Xu Y. Effects of ambient temperature and irradiance on performance of half-cut and shingled photovoltaic modules. Opt Precis Eng. 2021;29(8):1782-1794. https://doi.org/10.37188/OPE.20212908.1782.

[16] Park J, Oh W, Park H, Jeong C, Choi B, Lee J. Analysis of solar cells interconnected by electrically conductive adhesives for high-density photovoltaic modules. Appl Surf Sci. 2019;484:732-739. https://doi.org/10.1016/j.apsusc.2019.03.307.

[17] Lisco F, Bukhari F, Jones LO, Law AM, Walls JM, Ballif C. ETFE and its role in the fabrication of lightweight c-Si solar modules. IEEE J Photovolt. 2023;13(3):349-354. https://doi.org/10.1109/JPHOTOV.2023.3242212.